

Quantifying bankfull flow width using preserved bar clinofolds from fluvial strata

Evan Greenberg¹, Vamsi Ganti^{1,2} and Elizabeth Hajek³

¹Department of Geography, University of California–Santa Barbara, Santa Barbara, California 93106, USA

²Department of Earth Science, University of California–Santa Barbara, Santa Barbara, California 93106, USA

³Department of Geosciences, The Pennsylvania State University, University Park, Pennsylvania 16802, USA

ABSTRACT

Reconstruction of active channel geometry from fluvial strata is critical to constrain the water and sediment fluxes in ancient terrestrial landscapes. Robust methods—grounded in extensive field observations, numerical simulations, and physical experiments—exist for estimating the bankfull flow depth and channel-bed slope from preserved deposits; however, we lack similar tools to quantify bankfull channel widths. We combined high-resolution lidar data from 134 meander bends across 11 rivers that span over two orders of magnitude in size to develop a robust, empirical relation between the bankfull channel width and channel-bar clinofold width (relict stratigraphic surfaces of bank-attached channel bars). We parameterized the bar cross-sectional shape using a two-parameter sigmoid, defining bar width as the cross-stream distance between 95% of the asymptotes of the fit sigmoid. We combined this objective definition of the bar width with Bayesian linear regression analysis to show that the measured bankfull flow width is 2.34 ± 0.13 times the channel-bar width. We validated our model using field measurements of channel-bar and bankfull flow widths of meandering rivers that span all climate zones ($R^2 = 0.79$) and concurrent measurements of channel-bar clinofold width and mud-plug width in fluvial strata ($R^2 = 0.80$). We also show that the transverse bed slopes of bars are inversely correlated with bend curvature, consistent with theory. Results provide a simple, usable metric to derive paleochannel width from preserved bar clinofolds.

INTRODUCTION

Reconstruction of formative channel geometry from fluvial strata is critical to constrain the ancient hydrology and terrestrial mass fluxes on Earth and other planets (e.g., Bhattacharya et al., 2016), unravel fluvial responses to past climate change (Foreman et al., 2012), and aid hydrocarbon exploration (e.g., Miall and Tyler, 1991). Alluvial river geometry is characterized by streamwise channel-bed slope (S) and bankfull flow depth (h_{bf}) and width (B_{bf}). Robust methods—tested with extensive modern observations, numerical simulations, and physical experiments—exist for estimating h_{bf} and S from fluvial strata. For example, h_{bf} has been estimated from the geometry of preserved river dune deposits (Paola and Borgman, 1991; Leclair and Bridge, 2001; Jerolmack and Mohrig, 2005) or the preserved bar-clinofold surfaces (relict bank-attached and free channel-bar surfaces; Mohrig et al., 2000; Hajek and Heller, 2012; Alexander et al., 2020). Channel-bed slope has been estimated from the elevations

of correlative downstream channel architectures (Bhattacharya et al., 2016) or using empirical bankfull Shields stress criteria observed in modern rivers (Paola and Mohrig, 1996; Trampus et al., 2014). However, we lack similar tools to estimate B_{bf} from fluvial strata.

Current methods to reconstruct B_{bf} from fluvial strata leverage fully preserved channel architectures (Ielpi and Ghinassi, 2014), channel-belt dimensions (Gibling, 2006; Ielpi et al., 2017), and the scaling of B_{bf} and h_{bf} in extant rivers (Leeder, 1973; Hayden et al., 2019). Fully preserved abandoned channel fills offer a direct estimate of B_{bf} , but they are rarely preserved due to rechannelization or limited outcrop exposure (Bridge, 2003; Bhattacharya et al., 2016; Toonen et al., 2012). Abandoned channel dimensions can also be measured in seismic data sets (Bhattacharya et al., 2016) and on inverted topography where planform channel architecture is preserved at the terrestrial surface (Ielpi and Ghinassi, 2014). In the absence of these observations, B_{bf} is estimated from channel-body

widths, or in conjunction with estimated h_{bf} based on the width-to-depth scaling observed in modern alluvial rivers (Bridge, 2003; Hayden et al., 2019). These estimates are hampered by substantial uncertainty because channel-body dimensions can differ significantly from formative channel dimensions (Hayden et al., 2019), and the scaling between B_{bf} and h_{bf} depends on channel sinuosity (Bridge, 2003), varying by an order of magnitude in extant rivers (Trampus et al., 2014). While a more mechanistic method to estimate B_{bf} of single-threaded rivers exists (Lapôtre et al., 2019), it requires detailed measurements of bed and bank-material grain size and is yet to be expanded to include the cohesive effects of grain-size mixtures in the bank material and floodplain vegetation.

Following previous work (Allen, 1965; Ethridge and Schumm, 1978; Bridge, 2003; Bhattacharya et al., 2016), we propose that the geometry of meandering river channels is encoded in the size of bank-attached forced bars (point bars) and can be reconstructed from their deposits. Point bars are macroforms for which size scales with channel dimensions (Allen, 1965; Mohrig et al., 2000; Hajek and Heller, 2012). Point bar sediments can be readily identified in fluvial strata at outcrop scales (Fig. 1) and in seismic data (Jackson, 1976; Durkin et al., 2017), and their internal accretionary surfaces record lateral channel migration (Allen, 1965). Point bar deposits are also underrecognized in sandy deposits, suggesting a greater abundance of bar clinofold surfaces than is often considered (Hartley et al., 2015; Chamberlin and Hajek, 2019).

The ability to use preserved bar clinofolds as proxies for B_{bf} would unlock the potential for detailed morphodynamic reconstructions of ancient landscapes. We combined high-resolution topographic data from meandering rivers with Bayesian linear regression analysis

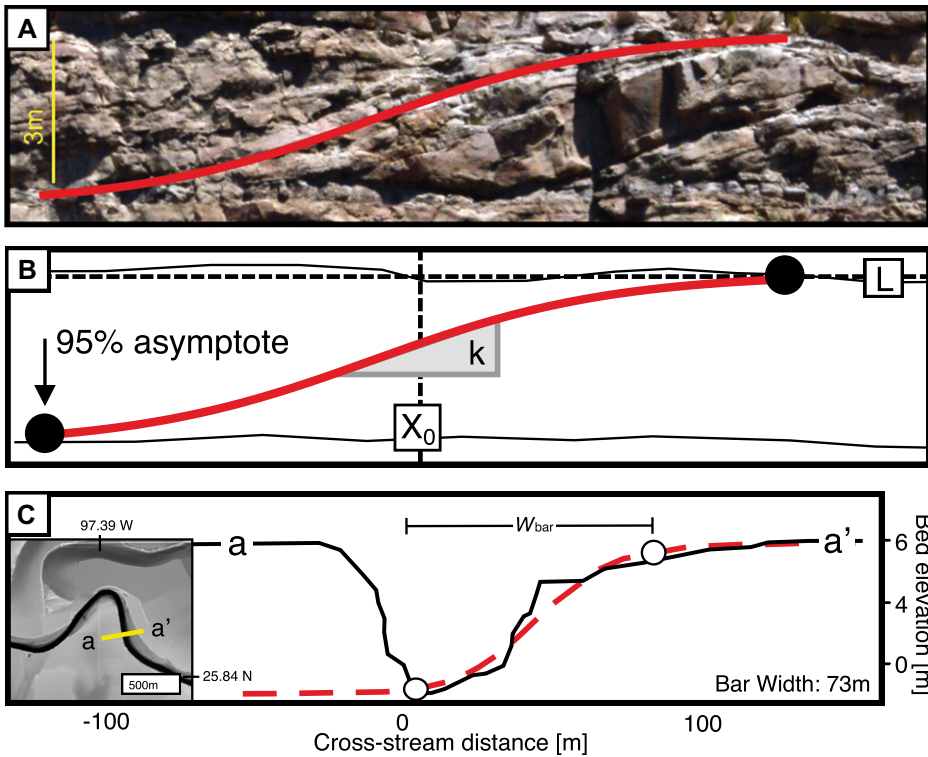


Figure 1. (A) Preserved bar clinoform surface (red line) from the Castlegate Formation, Utah, USA (Chamberlin and Hajek, 2019), and (B) fitted two-parameter sigmoid (Equation 1). (C) Example bathymetric cross section from the Rio Grande River, North America (inset shows location; Swartz et al., 2020), highlighting sigmoid (red dashed line) fit to point bar surface.

to develop a robust relation between B_{bf} and the point bar surface width, W_{bar} , which facilitates B_{bf} reconstruction from fluvial strata.

ANALYSIS OF MODERN RIVERS

We used lidar elevation data from 11 meandering rivers across the United States, available through OpenTopography (<https://opentopography.org>) (sampled at 1 m) and the U.S. Geological Survey (USGS) 3D Elevation Program (<https://www.usgs.gov/core-science-systems/ngp/3dep>) (sampled at 1 m and 1/3 arc-seconds; Fig. 2A). These rivers exhibit active channel migration and natural levee development and are not incised into their floodplains. Our data set spans bankfull depths of 2 m to 26 m (field estimates were available for nine reaches; the empirical relation of Ielpi and Lapôtre [2020] was used for h_{bf} estimation for two reaches) and reach lengths of 19 km to 183 km, and it covers six meander bends per study reach on average. The data set covers the temperate, arid, and cold Köppen climate classifications (Beck et al., 2018), bed slopes of 1×10^{-4} to 1×10^{-3} , and median discharges of 15 to 18,000 m³/s.

For each study reach, we mapped channel centerlines from Landsat 8 satellite imagery using RivaMap (Isikdogan et al., 2017). This method produced discontinuous centerlines when applied to rivers with small channel widths (<60 m) relative to the image resolution (30 m). We manually corrected all program-

matically generated centerlines to fill gaps and remove stems in the centerline from adjoining tributaries. We georeferenced the channel centerlines to the elevation products and systematically sampled each bend by generating at least three thalweg-perpendicular cross sections per bar at even spacing across the bend inlet, apex, and outlet (Fig. 2B). We computed B_{bf} as the cross-stream distance between manually picked channel levees (Fig. 2C).

The bases of the channel bars are perennially submerged, so we could not directly estimate W_{bar} from elevation data that did not penetrate water. To address this issue, we generated synthetic bathymetry below the hydroflattened water surface at every sampled location by linearly projecting the channel bank slopes until either the channel depth was equal to h_{bf} or the two channel-bank projections intersected (Fig. 2C). We validated this method with the Rio Grande, where both lidar and bathymetric cross-sectional data were available (Figs. 1C and 2C). To objectively define W_{bar} , we fit a two-parameter sigmoid to the cross-sectional shape of every sampled bar surface (Fig. 1):

$$f(x) = \frac{L}{1 + e^{k(x-x_0)}}, \quad (1)$$

where L and k are the sigmoid height and growth rate, respectively, x is the cross-stream location, and x_0 is the location of the bar inflection point

(Fig. 1B). We defined W_{bar} as the cross-stream distance between the locations that mark the 95% values of the asymptotes of the best-fitting sigmoid (Fig. 1B).

We propose a linear model given by

$$B_{bf} = \alpha W_{bar}, \quad (2)$$

where α is the regression slope, constrained by Bayesian linear regression. We evaluated α using individual cross-sectional measurements (W_{bar} , B_{bf}) and measurements aggregated at the bend scale and reach scale to generate a single value per bar (\overline{W}_{bar} , \overline{B}_{bf}) and river reach (\overline{W}_{bar} , \overline{B}_{bf} ; Fig. 2B), respectively. To validate the model, we compiled 10 previously reported B_{bf} and W_{bar} values from eight additional modern rivers and a numerically simulated meandering river. We compared our model performance to established width-depth relations derived from modern rivers that employ power-law (Leeder, 1973) and linear (Hayden et al., 2019) scaling, which are currently used to constrain B_{bf} from strata.

RESULTS

We made 424 independent paired measurements of (W_{bar} , B_{bf}) across 134 meander bends (Fig. 2). At a 95% high probability density interval, we found (Fig. 3A)

$$B_{bf} = (2.34 \pm 0.13)W_{bar}. \quad (3)$$

Results did not significantly change when data were aggregated at the bend ($\alpha = 2.18 \pm 0.16$) or reach scale ($\alpha = 2.18 \pm 0.36$). Bankfull channel width predicted with Equation 3 showed good agreement with the measured B_{bf} at the cross-sectional ($R^2 = 0.64$), bend-averaged ($R^2 = 0.73$), and reach-averaged ($R^2 = 0.93$) scales (Fig. 3B). The posterior predictive distribution of B_{bf} , at a 95% confidence for the individual cross-sectional data, was bounded by (Fig. 3A)

$$1.0W_{bar} \leq B_{bf} \leq 5.9W_{bar}. \quad (4)$$

Our model (Equation 3) predicted B_{bf} for the compiled natural and numerical rivers ($R^2 = 0.79$; Fig. 3D) and performed significantly better than the existing power-law ($R^2 = 0.55$) and linear ($R^2 = 0.23$) width-to-depth scaling relations. Furthermore, the order-of-magnitude uncertainty range in the width-to-depth scaling relations is significantly greater than both the high probability density interval and the posterior predictive interval (Equations 3 and 4) used in our method.

APPLICATION TO FLUVIAL STRATA

To test the model's applicability to ancient strata, we compiled paired measurements of fully preserved bar clinoform widths and mud-plug widths from four published outcrop panels and

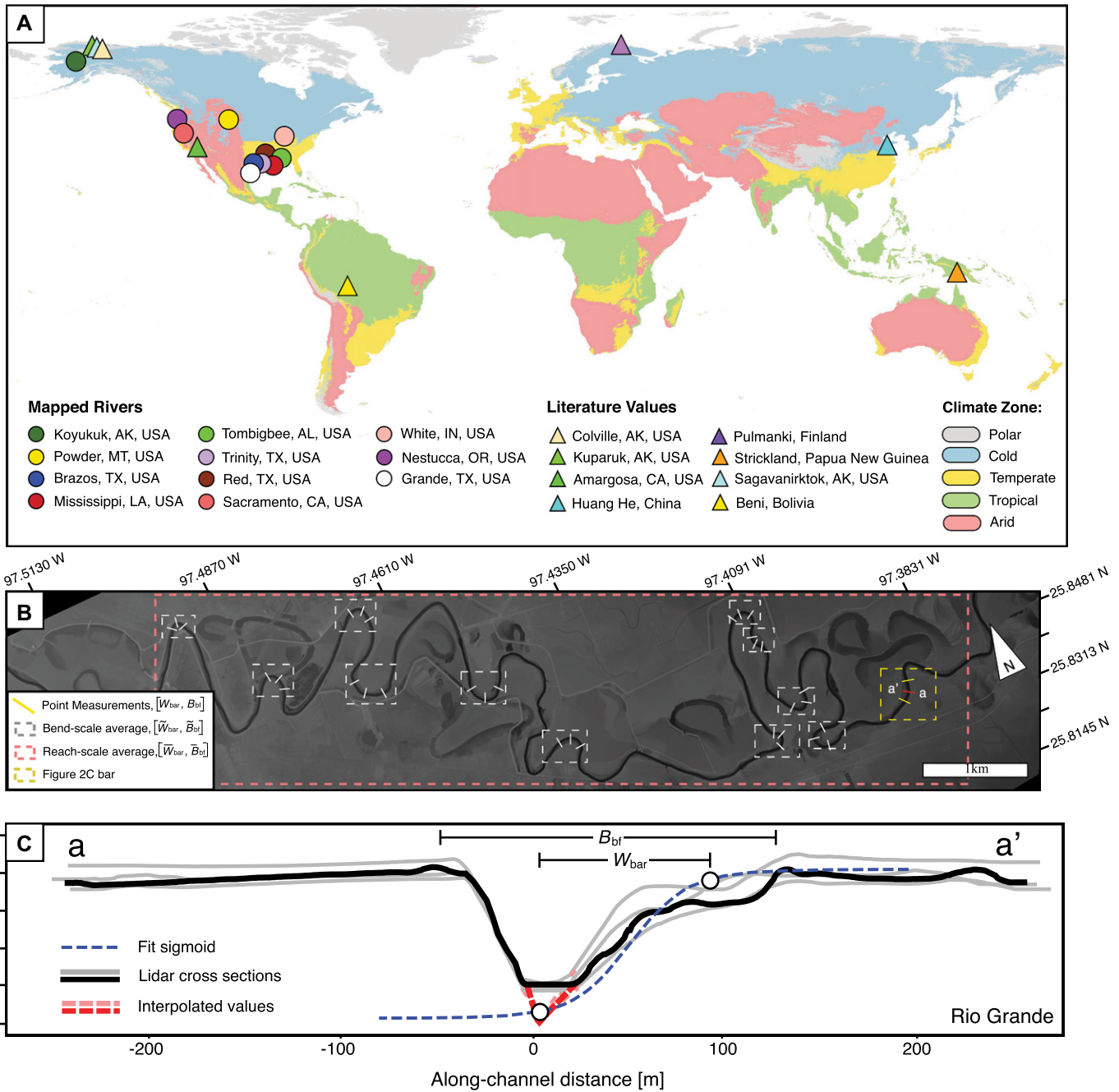


Figure 2. (A) Locations of bar width, W_{bar} , and bankfull flow width, B_{bf} , data overlain on a map of Köppen climate classifications (Beck et al., 2018). Circular and triangular markers indicate river reaches with lidar data and field measurements from previous studies, respectively. **(B)** Differences between cross-sectional, bend-, and reach-scale measurements of W_{bar} and B_{bf} highlighted using the Rio Grande River (North America). **(C)** Example cross sections (gray lines) from a Rio Grande meander bend, outlining the extrapolation scheme used to generate synthetic bathymetry (red line) below the hydroflattened water surface in lidar data (black line). Cross sections were aligned to match their lowest interpolated point.

two published seismic cross sections (details are provided in the Supplemental Material¹). From these six images, we independently estimated B_{bf} from the lateral extent of fully preserved abandoned channel fills. We measured W_{bar} from fully

¹Supplemental Material. River locations, data sources, regression results, full data, and extended methods. Please visit <https://doi.org/10.1130/GEOL.S.14470791> to access the supplemental material, and contact editing@geosociety.org with any questions.

preserved clinoforms that were correlative to the measured channel fills such that we sampled the same channel body (e.g., within the sixth-order bounding surfaces of Miall [1988]). We digitized the clinoform surfaces, fit Equation 1, and followed the same methodology applied to the modern bar surfaces to estimate W_{bar} .

Sample size, cross-section position relative to the bar apex, and the cross-section obliquity relative to the paleocurrent direction are factors that likely influence the application of our

model to fluvial strata. To test model sensitivity to these effects, we assumed that the bar clinoform preservation in fluvial strata is randomly distributed with respect to cross-section obliquity and bend position, and we generated channel cross sections at varying angles, θ , to the centerline direction across Trinity River (Texas, USA) bars, yielding a data set of channel cross sections at $\theta \in [0^\circ, 90^\circ]$. From this data set, we systematically sampled 1–15 cross sections at random angles and bend positions to assess

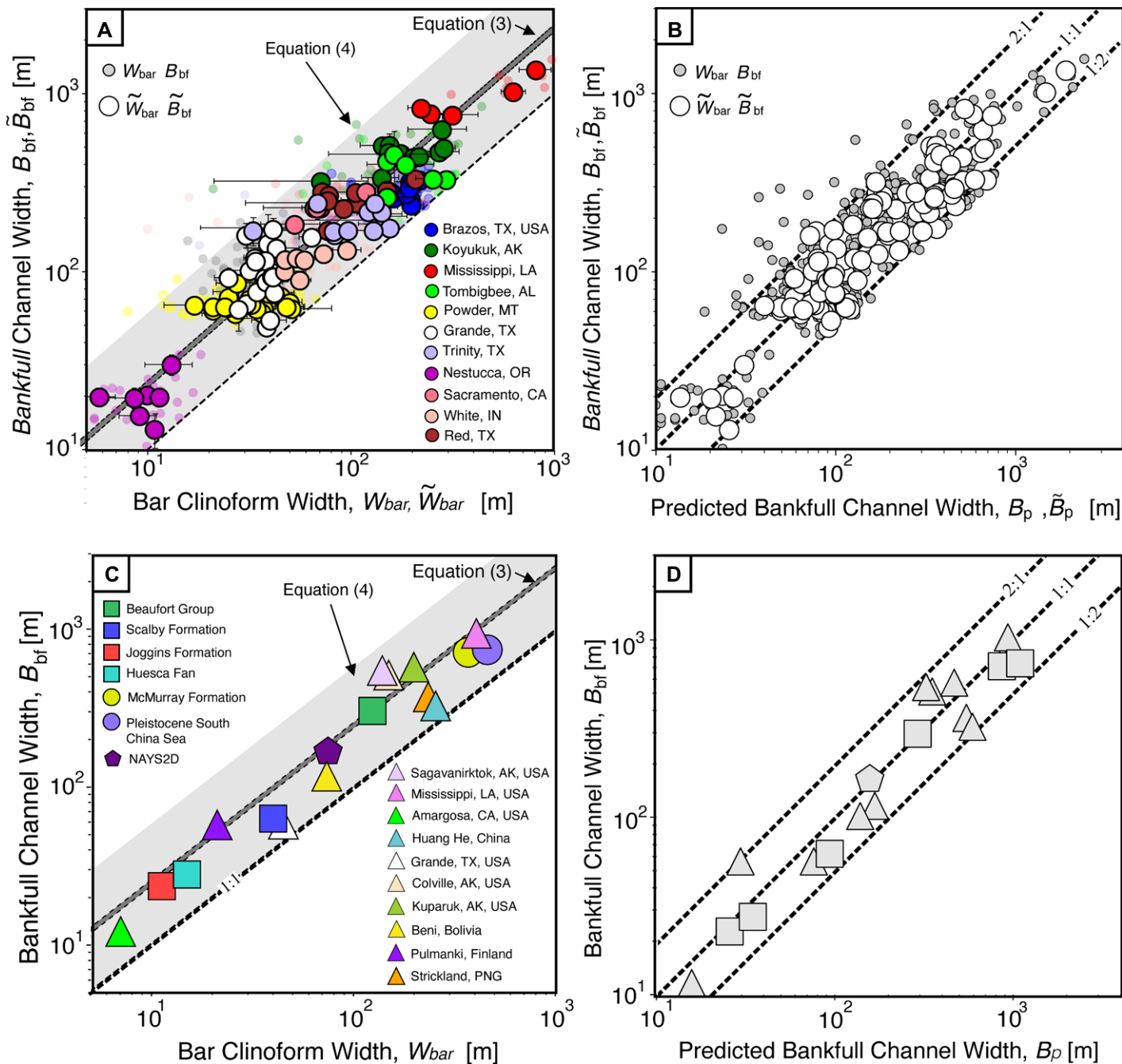


Figure 3. (A,C) Measured bankfull channel width as a function of estimated bar width for (A) cross-sectional and bend-scale observations from lidar data, and (C) previous observations from meandering rivers (triangles) and fluvial strata (squares). (B,D) Comparison of observed and model-predicted bankfull channel width for (B) lidar-derived observations, and (D) compiled observations from extant rivers and fluvial strata. Full data are reported in the Supplemental Material (see footnote 1).

sensitivity of α to sample size. We also sampled three cross sections at each θ to assess the sensitivity of α to θ .

Model predictions of B_{bf} using Equation 3 were consistent with the correlative measurements of abandoned channel widths ($R^2 = 0.80$; Fig. 3D), validating our model application to ancient strata. Our sensitivity tests revealed that a robust representation of W_{bar} and inferred B_{bf} from fluvial strata can be achieved by sampling ≥ 3 bar clinoforms from the same channel body (e.g., sixth-order bounding surfaces of

Miall, 1988; Fig. 4B). For cross sections with $\theta \lesssim 70^\circ$, α remained consistent (Fig. 4A) but never fully converged to Equation 3 (Fig. 4B). Multiple measurements from the same lateral accretion set (e.g., third-order bounding surfaces of Miall [1988], or multiple clinoform surfaces like those pictured in Fig. 1A) could be problematic because this violates the assumption of random bend positions. In the absence of multiple samples of preserved bar clinoforms across a channel complex, Equation 4 can be used to estimate B_{bf} from a single W_{bar} measurement that

has been geometrically corrected to paleoflow perpendicular direction. While our model is directly applicable to fully preserved clinoforms, the symmetry of Equation 1 may enable model application by fitting the sigmoid to a partially preserved bar clinoform, so long as at least half of the original bar surface is preserved.

DISCUSSION AND CONCLUSIONS

We present a robust method to estimate B_{bf} of meandering rivers from preserved point bar surfaces in fluvial strata. Using high-resolution lidar

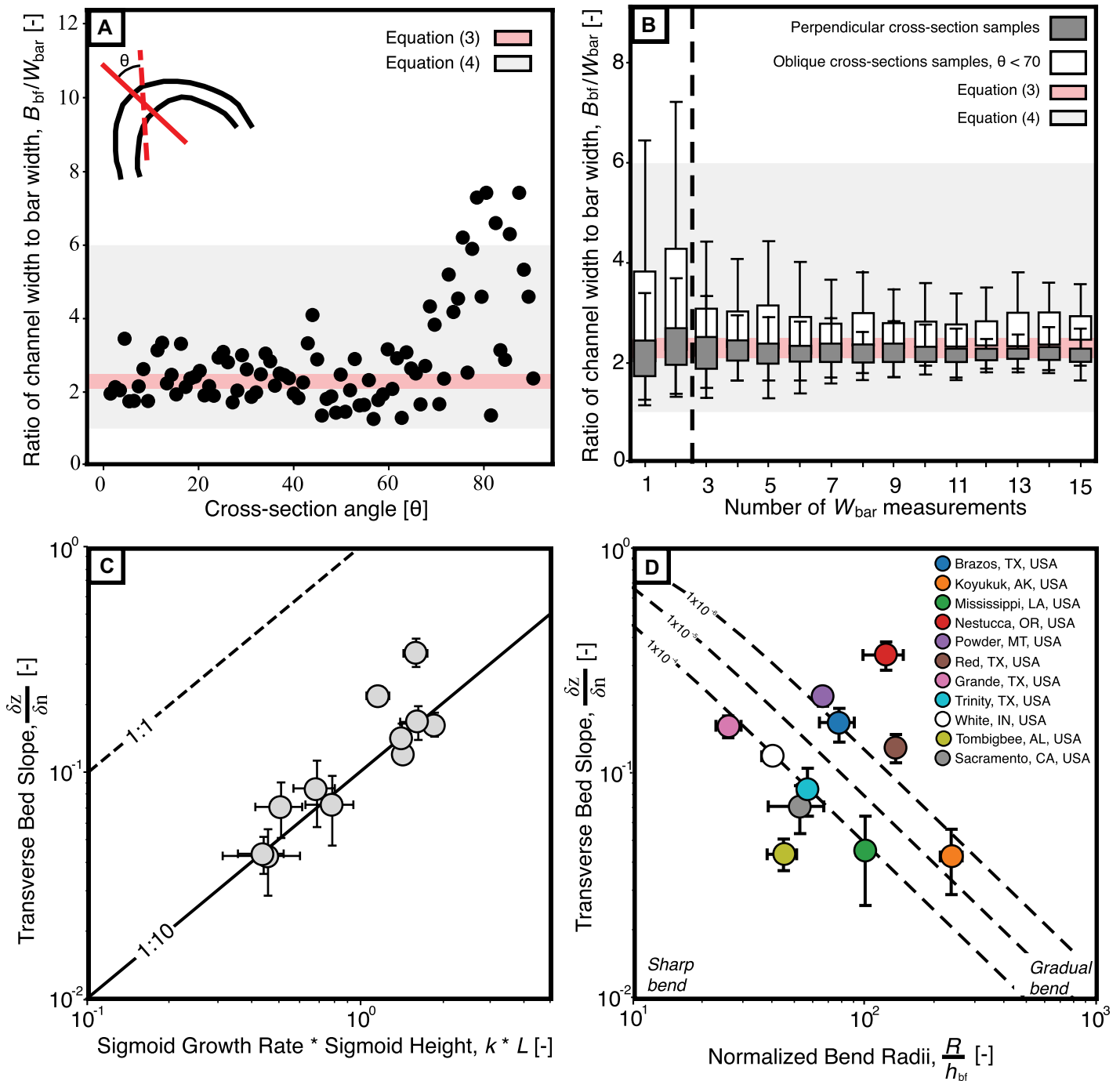


Figure 4. (A,B) Functional dependence of B_{bf}/W_{bar} on (A) cross-section obliquity angle, θ (see inset for definition), and (B) sample size per river bend of the Trinity River (Texas, USA). Markers in A represent the average of three samples of W_{bar} and B_{bf} for every value of θ . (C,D) Relationship between transverse bed slope of bar and (C) growth parameter, k , from Equation 1, averaged over the study reach, and (D) reach-scale average of bend radius normalized by bankfull flow depth, R/h_{bf} . Dotted lines indicate predictions at varying relative roughness (following Talmon et al., 1995).

data and field observations of W_{bar} and B_{bf} from 19 rivers, and concurrent field measurements of preserved bar clinoform width and mud-plug widths from fluvial strata, we showed that the formative channel width is $2.34 \pm 0.13 \times$ the measured channel-bar width. Our model is minimally sensitive to sample size and the position and angle of the preserved bar clinoforms with respect to the paleocurrent direction (Figs. 4A and 4B). These results enable the robust inver-

sion of B_{bf} from fluvial strata and confirm previously proposed heuristic relations between W_{bar} and B_{bf} (Ethridge and Schumm, 1978; Bhattacharya et al., 2016). The consistency between the predicted channel width and measured mud-plug widths (Fig. 3D) indicates that Equation 3 can substantially reduce uncertainty in ancient B_{bf} estimates compared to existing methods. While Equation 4 provides a lower-precision estimate of B_{bf} when limited samples are avail-

able from fluvial strata, the credible interval is of higher precision than the indirect methods based on h_{bf} . Further, our model can also be used to estimate B_{bf} from bar clinoforms documented in Martian fluvial strata (Goudge et al., 2018).

We also explored the controls on the variability of bar shapes between rivers. In Equation 1, L is set by h_{bf} , and we found that k is related to the transverse bed slope of bars, $\partial z/\partial n$ (Fig. 4C). Theoretical, experimental, and field studies

have explored the controls on $\partial z/\partial n$ (Struiksma et al., 1985; Talmon et al., 1995), and our results revealed that $\partial z/\partial n$ averaged across the bars of the individual study reaches is inversely proportional to their radius of curvature relative to channel depth (Fig. 4D), consistent with theory. While cross-section position relative to the channel apex will directly influence $\partial z/\partial n$ (Kleinhaus et al., 2012), this observation suggests that quantitative characterization of bar cliniform shape (Eq. 1) may enable the comparison of average bend curvatures across paleochannels.

Finally, quantification of preserved bar deposit and paleochannel widths can enable reconstructions of paleoriver mobility. Robust B_{br} estimates can inform empirical relations between channel width and the lateral migration rates of meandering rivers (Ielpi and Lapôte, 2020). Equation 1 can also be used to quantify the extent of vertical preservation of formative bar topography, which encodes the relative time scales of channel migration and avulsion (Chamberlin and Hajek, 2019; Ganti et al., 2020). Thus, detailed measurements of the size and shape of preserved bars in fluvial strata can constrain the geometry and rates of ancient river evolution, which are central to unraveling fluvial responses to boundary condition perturbations on Earth and river mobility on Mars.

ACKNOWLEDGMENTS

We thank A. Ielpi and two anonymous reviewers for constructive feedback. This work was supported by National Science Foundation grants to Ganti (EAR 1935669) and Hajek (EAR 1935513).

REFERENCES CITED

- Alexander, J.S., McElroy, B.J., Huzurbazar, S., and Murr, M.L., 2020, Elevation gaps in fluvial sandbar deposition and their implications for paleodepth estimation: *Geology*, v. 48, p. 718–722, <https://doi.org/10.1130/G47521.1>.
- Allen, J.R.L., 1965, The sedimentation and palaeogeography of the Old Red Sandstone of Anglesey, North Wales: *Proceedings of the Yorkshire Geological Society*, v. 35, p. 139–185, <https://doi.org/10.1144/pygs.35.2.139>.
- Beck, H., Zimmermann, N., McVicar, T., Vergopolan, N., Berg, A., and Wood, E., 2018, Present and future Köppen-Geiger climate classification maps at 1-km resolution: *Scientific Data*, v. 5, 180214, <https://doi.org/10.1038/sdata.2018.214>.
- Bhattacharya, J.P., Copeland, P., Lawton, T.F., and Holbrook, J., 2016, Estimation of source area, river paleo-discharge, paleoslope, and sediment budgets of linked deep-time depositional systems and implications for hydrocarbon potential: *Earth-Science Reviews*, v. 153, p. 77–110, <https://doi.org/10.1016/j.earscirev.2015.10.013>.
- Bridge, J.S., 2003, *Rivers and Floodplains: Forms, Processes, and Sedimentary Record*: New York, Wiley-Blackwell, 504 p.
- Chamberlin, E.P., and Hajek, E.A., 2019, Using bar preservation to constrain reworking in channel-dominated fluvial stratigraphy: *Geology*, v. 47, p. 531–534, <https://doi.org/10.1130/G46046.1>.
- Durkin, P.R., Boyd, R.L., Hubbard, S.M., Shultz, A.W., and Blum, M.D., 2017, Three-dimensional reconstruction of meander-belt evolution, Cretaceous McMurray Formation, Alberta Foreland Basin, Canada: *Journal of Sedimentary Research*, v. 87, no. 10, p. 1075–1099, <https://doi.org/10.2110/jsr.2017.59>.
- Ethridge, R.G., and Schumm, S., 1978, Reconstructing paleochannel morphologic and flow characteristics: Methodology, limitations, and assessment, in Miall, A.D., ed., *Fluvial Sedimentology*: Canadian Society Petrology Geology Memoir 5, p. 703–721.
- Foreman, B.Z., Heller, P.L., and Clementz, M.T., 2012, Fluvial response to abrupt global warming at the Palaeocene/Eocene boundary: *Nature*, v. 491, p. 92–95, <https://doi.org/10.1038/nature11513>.
- Ganti, V., Hajek, E.A., Leary, K., Straub, K.M., and Paola, C., 2020, Morphodynamic hierarchy and the fabric of the sedimentary record: *Geophysical Research Letters*, v. 47, e2020GL087921, <https://doi.org/10.1029/2020gl087921>.
- Gibling, M.R., 2006, Width and thickness of fluvial channel bodies and valley fills in the geological record: A literature compilation and classification: *Journal of Sedimentary Research*, v. 76, p. 731–770, <https://doi.org/10.2110/jsr.2006.060>.
- Goudge, T.A., Mohrig, D., Cardenas, B.T., Hughes, C.M., and Fassett, C.I., 2018, Stratigraphy and paleohydrology of delta channel deposits, Jezero crater, Mars: *Icarus*, v. 301, p. 58–75, <https://doi.org/10.1016/j.icarus.2017.09.034>.
- Hajek, E.A., and Heller, P.L., 2012, Flow-depth scaling in alluvial architecture and nonmarine sequence stratigraphy: Example from the Castlegate Sandstone, central Utah, U.S.A.: *Journal of Sedimentary Research*, v. 82, p. 121–130, <https://doi.org/10.2110/jsr.2012.8>.
- Hartley, A.J., Owen, A., Swan, A., Weissmann, G.S., Holzweber, B.I., Howell, J., Nichols, G., and Scuderi, L., 2015, Recognition and importance of amalgamated sandy meander belts in the continental rock record: *Geology*, v. 43, p. 679–682, <https://doi.org/10.1130/G36743.1>.
- Hayden, A.T., Lamb, M.P., Fischer, W.W., Ewing, R.C., McElroy, B.J., and Williams, R.M.E., 2019, Formation of sinuous ridges by inversion of river-channel belts in Utah, USA, with implications for Mars: *Icarus*, v. 332, p. 92–110, <https://doi.org/10.1016/j.icarus.2019.04.019>.
- Ielpi, A., and Ghinassi, M., 2014, Planform architecture, stratigraphic signature and morphodynamics of an exhumed Jurassic meander plain (Scalby Formation, Yorkshire, UK): *Sedimentology*, v. 61, p. 1923–1960, <https://doi.org/10.1111/sed.12122>.
- Ielpi, A., and Lapôte, M.G.A., 2020, A tenfold slowdown in river meander migration driven by plant life: *Nature Geoscience*, v. 13, p. 82–86, <https://doi.org/10.1038/s41561-019-0491-7>.
- Ielpi, A., Rainbird, R.H., Ventra, D., and Ghinassi, M., 2017, Morphometric convergence between Proterozoic and post-vegetation rivers: *Nature Communications*, v. 8, p. 1–8, <https://doi.org/10.1038/ncomms15250>.
- Isikdogan, F., Bovik, A., and Passalacqua, P., 2017, RivaMap: An automated river analysis and mapping engine: *Remote Sensing of Environment*, v. 202, p. 88–97, <https://doi.org/10.1016/j.rse.2017.03.044>.
- Jackson, R.G., 1976, Depositional model of point bars in the Lower Wabash River: *Journal of Sedimentary Research*, v. 46, p. 579–594.
- Jerolmack, D.J., and Mohrig, D., 2005, A unified model for subaqueous bed form dynamics: *Water Resources Research*, v. 41, W12421, <https://doi.org/10.1029/2005WR004329>.
- Kleinhaus, M.G., Haas, T., Lavoie, E., and Makaske, B., 2012, Evaluating competing hypotheses for the origin and dynamics of river anastomosis: *Earth Surface Processes and Landforms*, v. 37, p. 1337–1351, <https://doi.org/10.1002/esp.3282>.
- Lapôte, M.G., Ielpi, A., Lamb, M.P., Williams, R.M., and Knoll, A.H., 2019, Model for the formation of single-thread rivers in barren landscapes and implications for pre-Silurian and Martian fluvial deposits: *Journal of Geophysical Research: Earth Surface*, v. 124, p. 2757–2777, <https://doi.org/10.1029/2019JF005156>.
- Leclair, S.F., and Bridge, J.S., 2001, Quantitative interpretation of sedimentary structures formed by river dunes: *Journal of Sedimentary Research*, v. 71, p. 713–716, <https://doi.org/10.1130/2DC40962-0E47-11D7-8643000102C1865D>.
- Leeder, M.R., 1973, Fluvial fining-upwards cycles and the magnitude of palaeochannels: *Geological Magazine*, v. 110, p. 265–276, <https://doi.org/10.1017/S0016756800036098>.
- Miall, A.D., 1988, Architectural elements and bounding surfaces in fluvial deposits: Anatomy of the Kayenta Formation (Lower Jurassic): Southwest Colorado: *Sedimentary Geology*, v. 55, p. 233–262, [https://doi.org/10.1016/0037-0738\(88\)90133-9](https://doi.org/10.1016/0037-0738(88)90133-9).
- Miall, A.D., and Tyler, N., eds., 1991, *The Three-Dimensional Facies Architecture of Terrigenous Clastic Sediments and its Implications for Hydrocarbon Discovery and Recovery*: Society for Sedimentary Geology (SEPM) Concepts in Sedimentology and Paleontology 3, 309 p., <https://doi.org/10.2110/csp.91.03>.
- Mohrig, D., Heller, P.L., Paola, C., and Lyons, W.J., 2000, Interpreting avulsion process from ancient alluvial sequences: Guadalupe-Matarranya system (northern Spain) and Wasatch Formation (western Colorado): *Geological Society of America Bulletin*, v. 112, p. 1787–1803, [https://doi.org/10.1130/0016-7606\(2000\)112<1787:IA PFAA>2.0.CO;2](https://doi.org/10.1130/0016-7606(2000)112<1787:IA PFAA>2.0.CO;2).
- Paola, C., and Borgman, L., 1991, Reconstructing random topography from preserved stratification: *Sedimentology*, v. 38, p. 553–565, <https://doi.org/10.1111/j.1365-3091.1991.tb01008.x>.
- Paola, C., and Mohrig, D., 1996, Palaeohydrodynamics revisited: Palaeoslope estimation in coarse-grained braided rivers: *Basin Research*, v. 8, p. 243–254, <https://doi.org/10.1046/j.1365-2117.1996.00253.x>.
- Struiksma, N., Olesen, K.W., Flokstra, C., and De Vriend, H.J., 1985, Bed deformation in curved alluvial channels: *Journal of Hydraulic Research*, v. 23, p. 57–79, <https://doi.org/10.1080/00221688509499377>.
- Swartz, J.M., Goudge, T.A., and Mohrig, D.C., 2020, Quantifying coastal fluvial morphodynamics over the last 100 years on the Lower Rio Grande, USA and Mexico: *Journal of Geophysical Research: Earth Surface*, v. 125, <https://doi.org/10.1029/2019JF005443>.
- Talmon, A.M., Struiksma, N., and Van Mierlo, M.C.L.M., 1995, Laboratory measurements of the direction of sediment transport on transverse alluvial-bed slopes: *Journal of Hydraulic Research*, v. 33, p. 495–517, <https://doi.org/10.1080/00221689509498657>.
- Toonen, W.H.J., Kleinhaus, M.G., and Cohen, K.M., 2012, Sedimentary architecture of abandoned channel fills: *Earth Surface Processes and Landforms*, v. 37, p. 459–472, <https://doi.org/10.1002/esp.3189>.
- Trampush, S.M., Huzurbazar, S., and McElroy, B., 2014, Empirical assessment of theory for bankfull characteristics of alluvial channels: *Water Resources Research*, v. 50, p. 9211–9220, <https://doi.org/10.1002/2014WR015597>.

Printed in USA